Shortened version of the paper published in ASTRONOMY LETTERS, 2002, Vol. 28, No. 8, p. 495–508

A COLD FRONT IN A3667: HYDRODYNAMICS AND MAGNETIC FIELD IN THE INTRACLUSTER MEDIUM

A. Vikhlinin[1,2], M. Markevitch[2],

[1] *Institute for Space Research, Moscow, Russia*
[2] *Harvard-Smithsonian Center for Astrophysics*

This conference presentation discusses a *Chandra* observation of the cold front in Abell 3667. We first review our earlier results which include a measurement of the front velocity, $M \approx 1$, using the ratio of exterior and interior gas pressures; observations of the hydrodynamic effects expected for a transonic front motion (weak bow shock and gas compression near the leading edge of the front); direct observation of the suppressed diffusion across the front, and estimate of the magnetic field strength near the front from suppression of the Kelvin-Helmholtz instabilities.

The new results include using the 2-dimensional brightness distribution inside the cold front (a) to show that the front is stable and (b) to map the mass distribution in the gas cloud. This analysis confirms the existence of a dark matter subcluster traveling with the front. We also fix an algebraic error in our published calculations for the growth rate of the KH instability and discuss an additional effect which could stabilize the front against the small-scale perturbations. These updates only strengthen our conclusions regarding the importance of the magnetic fields for the front dynamics.

A3667 shows clear signs of the on-going merger of two big subclusters in its optical, X-ray, and radio images (Sodre et al. 1992, Knopp et al. 1996, Röttgering et al. 1997). The optical image contains two distinct galaxy concentrations around the giant elliptical galaxies (we call them A and B); the weak lensing observations reveal the associated mass concentrations (Joffre et al. 2000). The X-ray emission is elongated and co-aligned with the galaxy distribution. The most striking feature in the X-ray image is a strong surface brightness edge to the South-East of galaxy A, located perpendicularly to the A-B axis. The radio map reveals giant diffuse source of a 0.5–1 Mpc size, located in the cluster outskirts and oriented perpendicularly to the A-B axis. All available data point to identification of galaxies A and B as the centers of the two merging sublclusters. Although it is expected that sublusters should move supersonically ($v = 2000 - 3000$ km Ó$^{-1}$) during the merger, the observed line-of-sight velocity difference of galaxies A and B is only 120 km s^{-1} (Katgert et al. 1998). This means that the merger axis is perpendicular to the line of sight, which significantly simplifies interpretation of the data.

In this conference paper, we first review some earlier results from the *Chandra* observation of A3667 presented in Vikhlinin et al. (2001ab). We also present new results on mapping of the dark mass of the subcluster traveling with the cold front. We also fix an algebraic error in the calculations for the growth rate of the KH instability and discuss an additional effect which could effectively stabilize the front against the small-scale perturbations.

CHANDRA OBSERVATION OF A3667

The central part of A3667 was observed by *Chandra* in late 1999. The field of view was centered on the surface brightness edge 8′ to the South-East of galaxy A. *Chandra* angular resolution of 1″ corresponds to a proper size of 1.46 kpc at the cluster redshift, $z = 0.055$ (we assume $H_0 = 50$ km s^{-1} Mpc^{-1} hereafter). The technical aspects of the *Chandra* data analysis are presented in Vikhlinin et al. (2001a).

The *Chandra* X-ray image in the 0.7–4 keV energy band in shown in Fig. 1. Figure 2 shows its slightly smoothed version with the main structures marked. The most prominent feature is a sharp surface brightness edge whose shape is circular with a radius of 410 ± 15 kpc. The edge is very sharp — it is unresolved even with *Chandra*'s angular resolution.

The temperature map is presented on the bottom panel of Fig. 1. All variations of the temperature in region to the North-West of the edge, where the surface brightness is high, are significant. To the South-East of the edge the surface brightness is low and the temperature uncertainties are quite large. The very hot spots ($T > 12$ keV) are statistically insignificant. However, it is very clear that the gas temperature exterior to the edge is much higher than that inside. Such structures, observed previously in A2142 (Markevitch et al. 2001) were termed the "cold fronts".

To the South of the cold front, there is a second, weaker surface brightness discontinuity clearly visible in the smoothed image (Fig. 2). We discuss below that this structure can be associated with the bow shock in front of the cold cloud moving at a slightly supersonic speed.

A quantitative study of the cold front properties can be made using the observed X-ray surface brightness and temperature profiles across the front (Fig. 3). The brightness profile shows a sharp discontinuity. The brightness increases by a factor of two within 7–10 kpc of the front position and gradually increases by another factor of 2 within 40–80 kpc. Such a shape is typical for the projected spherical density discontinuity. The deprojection of the surface brightness profile gives the gas density $n_e =$

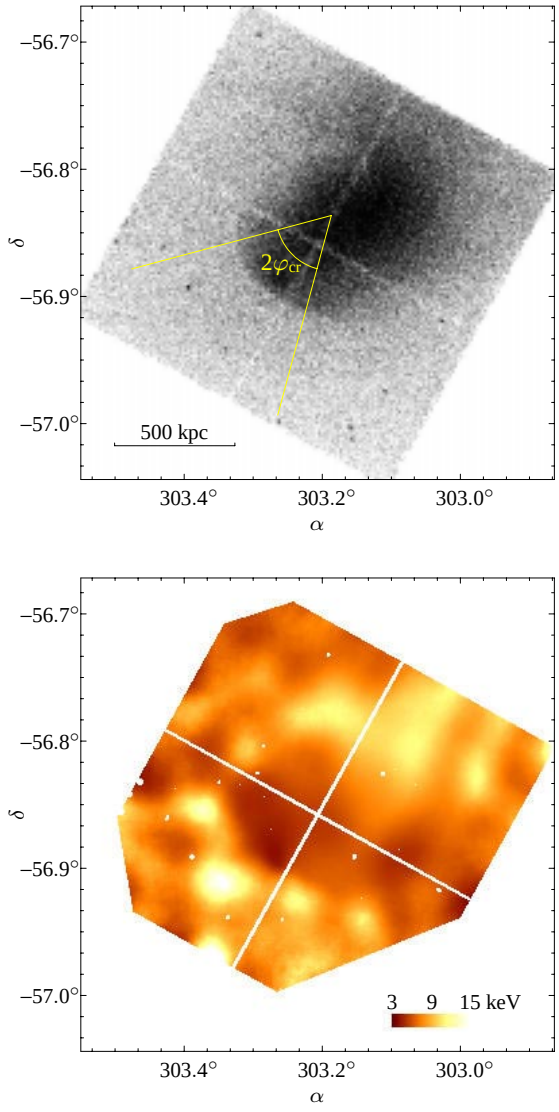

Fig. 1. *Chandra* X-ray image and temperature map of A3667. Note that the surface brightness edge (cold front) is very sharp within the sector $2\varphi_{cr} = 60°$, beyond which it is gradually smeared out.

$(3.2 \pm 0.48) \times 10^{-3}\,\mathrm{cm}^{-3}$ interior to the front, where the error bars conservatively include both measurement and all systematic uncertainties. Exterior to the front, the gas density is $n_e = 0.82 \times 10^{-3}\,\mathrm{cm}^{-3}$.

Across the front, the temperature changes sharply from ~ 8 to 4.5 keV (Fig. 3). The measured temperatures on both sides are consistent with constant values within some distance from the front. The average temperature within 275 kpc exterior to the front is $T_{\rm out} = 7.7 \pm 0.8$ keV, and within 125 kpc interior to the front it is $T_{\rm in} = 4.1 \pm 0.2$ keV.

Therefore, both gas density and temperature undergo a jump across the surface brightness edge. The corresponding pressure ratio is $p_{\rm in}/p_{\rm out} = 2.1 \pm 0.5$ (Table 1), with a rather conservative errorbar. If the cold front were at rest, there would be a pressure equilibrium, $p_{\rm in} = p_{\rm out}$. The higher inner pressure means that the front is moving and therefore the interior gas "feels" both the thermal and ram pressure of the exterior gas.

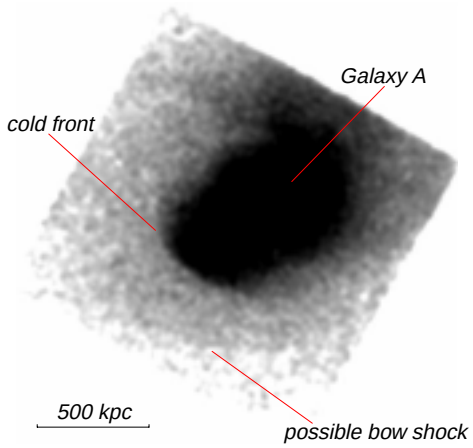

Fig. 2.

HYDRODYNAMICS NEAR THE COLD FRONT

The observed ram pressure leads to a rather accurate measurement of the front velocity, $M_1 = 1.0 \pm 0.2$, i.e. the gas cloud moving at the sound speed of the hotter gas. The cloud velocity in physical units is $v = 1430 \pm 290$ km s^{-1}.

Since the cold front moves with a velocity close to the speed of sound, the compressibility of the gas should be important and therefore two additional structures can be expected, and indeed observed (Vikhlinin et al. 2001a): a) surface brightness enhancement due to gas compression near the leading edge of the body, and b) a bow shock if the front velocity is even slightly supersonic.

Is the front shape stable?

In the discussion above, we implicitly assumed that the front moves as a solid body. Can the assumption of the constant front shape be justified? If the hydrodynamic instabilities[1] are allowed to operate freely, they significantly disturb (and even destroy) a gas cloud of radius R by the time it travels a distance of several R's (Jones et al. 1996). Since we observe a very regular shape of the leading edge of the cold front, this suggests that the instabilities should be somehow suppressed.

Another indication of the constancy of the front shape can be obtained by considering a dependence of gas pressure on angle from the direction of motion. All flow lines in the immediate vicinity of the front pass through a very small region near the leading edge. If the front shape is constant, the flow is stationary and therefore the gas pressure should follow the Bernoulli equation — the pressure decreases as the flow accelerates away from the stagnation

[1] In this case the most important type of instability is Rayleigh-Taylor

Table 1. Gas parameters near the cold front in A3667

Region	T keV	n_e 10^{-3} cm^{-3}	$p = Tn_e$ 10^{-2} keV cm^{-3}
Exterior	7.7 ± 0.8	0.82 ± 0.12	0.63 ± 0.11
Interior	4.1 ± 0.2	3.2 ± 0.5	1.32 ± 0.21

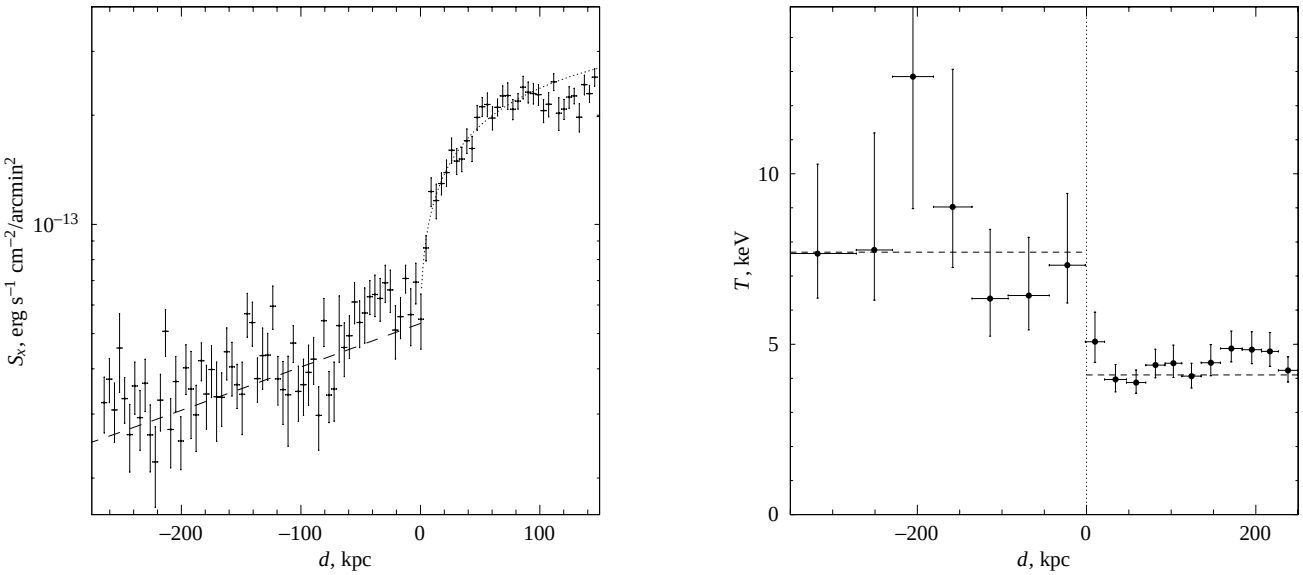

Fig. 3. X-ray surface brightness and temperature profiles across in the $\pm 15^\circ$ sector across the front. The dashed line in the left panel corresponds to the *ROSAT* profile without any renormalization. The dotted line corresponds to projection of the spherical density discontinuity.

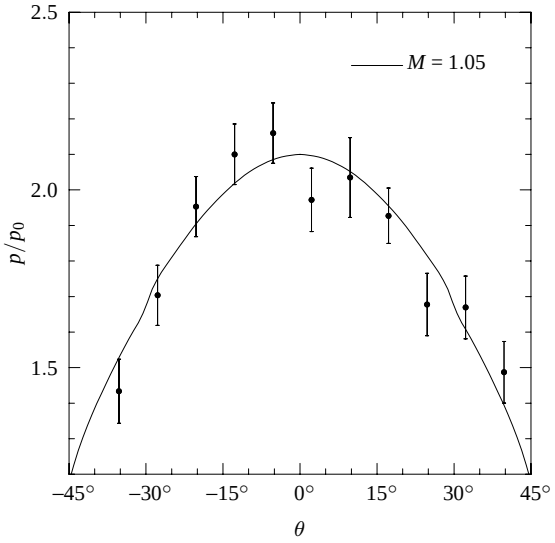

Fig. 4. Gas pressure inside the front as a function of angle from the leading edge. The line is not the fit, but prediction for the $M = 1.05$ flow.

region. The pressure inside the front should correspond to the exterior pressure, otherwise the shape will change and flow will not be stationary. Therefore, the assumption of the constant front shape leads to an easy and verifiable prediction of the interior pressure distribution as a function of angle from the direction of motion.

To determine the distribution of gas pressure, we need to measure both gas density and temperature as a function of angle, θ. We find that $T = 3.8 \pm 0.40$ keV in the $-10^\circ < \theta < 10^\circ$ sector relative to the motion direction, 3.8 ± 0.55 keV in the $-30^\circ < \theta < -10^\circ$ sector, and 4.7 ± 0.70 keV for $10^\circ < \theta < 30^\circ$.[2] Within the uncertainties, these values agree with the mean temperature inside the front $T = 4.1 \pm 0.2$ keV (Table 1), therefore we assume that the interior gas temperature is constant as a function of angle.

Given the constant temperature, the pressure is simply proportional to the gas density which is easily derived from deprojection of the surface brightness profiles across the front in different sectors from the direction of motion. The resulting angular dependence of the gas pressure in shown in Fig. 4. The pressure significantly declines — by a factor of 1.5 — at $\theta = 30^\circ$, where the front starts to widen. Remarkably, the numerical gasdynamic solution (using the VH-1 code) for the flow about the solid body at Mach numbers just above 1 predicts just such a change in pressure (solid line in Fig. 4). Thus, the angular dependence of the interior gas pressure at least implicitly confirms that the front moves with a constant shape.

Note that if we can assume *a priori* that the front shape is stable and the gas temperature inside is uniform, the dependence $p(\theta)$ is a convenient diagnostics of the front speed. Indeed, $p(\theta)$ is rather sensitive to the flow speed; for example, the shape of the measured angular dependence of pressure shown in Fig. 4 can be reproduced only for $0.7 < M < 1.5$. Under the assumption of constant temperature, $p(\theta)$ is equivalent to $\rho(\theta)/\rho(0)$, which is easily derived from the imaging data only.

Dark halo associated with the cold front

Since the shape of the cold front remains constant, we can naturally assume that the interior gas is in hydrostatic equilibrium in the gravitational field in its reference frame. In this case, the hydrostatic equilibrium equation, which under assumption of constant temperature reduces to

$$\rho = \rho_0 \exp(-\mu m_p \varphi / T), \qquad (1)$$

[2] The spectra were collected from a 70 kpc strip just inside the front; angles are front North to South through East

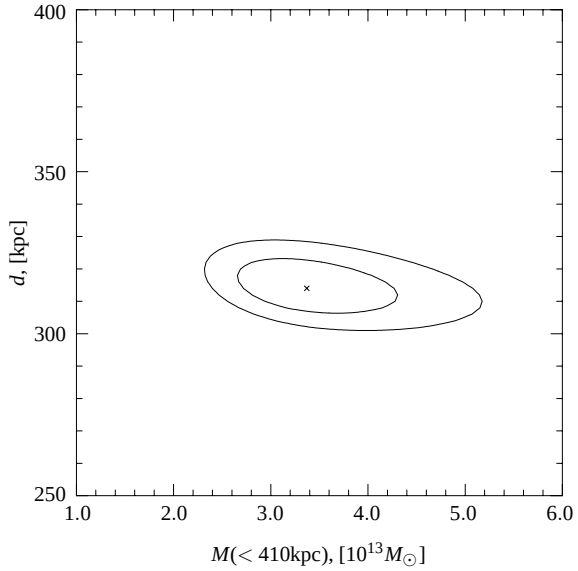

Fig. 5. Confidence intervals(68% and 95%) for location of the centroid of the King profile d (distance from the center of curvature of the cold front), and total mass within r = 410 kpc.

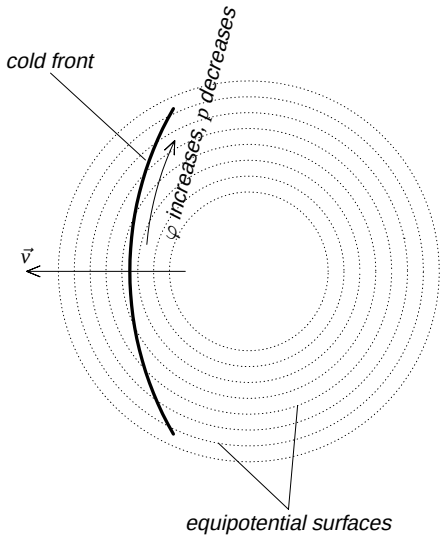

Fig. 6.

allows to infer the distribution of mass of the subcluster traveling with the front. We assume that the subcluster dark matter density profile is given by the King profile, $\rho_m = \rho_{m0}(1+r^2/r_c^2)^{-3/2}$. The density distribution of the cold gas is then given by equation (1) where $\varphi = 4\pi G\rho_0\left(1-\mathrm{asinh}\,x/x\right)$, denoting $x = r/r_c$. Integration of the plasma emissivity, $\varepsilon \propto \rho^2$, along the line of sight gives the model distribution of the surface brightness.

The maximum likelihood fit of this model to the observed 2-dimensional surface brightness distribution within approximately 200 kpc of the front gives the parameters of the King profile — the distance, d, of the dark halo centroid from the center curvature of the front, its core-radius r_c, and central density which we parameterize as the total mass within a sphere of the 410 kpc radius (the radius of the front). The fit is restricted to the region near the leading edge of the body due to the following reasons: 1) this region is most interesting from the point of view of the front dynamics; 2) we can reasonably assume that the gas distribution there is axially symmetric; 3) this region is small enough for the King profile to have sufficient freedom for approximating any reasonable distribution of mass.

The results of the maximum likelihood fitting are shown in Fig. 5. We find that the center of mass is located at $d = 315 \pm 7$ kpc from the center of curvature of the cold front (i. e. only at 95 kpc from the leading edge), and the total mass within 410 kpc is $(3.2 \pm 0.8) \times 10^{13} M_\odot$. The allowed values of the core-radius are in the range 50 kpc $< r_c <$ 200 kpc. Interestingly, the derived values of mass and core-radius are very reasonable for the central region of a 3–4 keV cluster. The total mass within a sphere of the 100 kpc radius (the distance to the front) is $4.6 \times 10^{12} M_\odot$, with exceeds the gas mass within the same radius by a factor of 15.

The distance from the subcluster center of mass to the leading edge of the front is only 25% of the front radius. This means, roughly speaking, that the dark matter halo moves in front of the cold gas and pulls it along. Note that such a configuration is required for the global stability of the front, as illustrated in Fig. 6. Indeed, in the absence of any gravitational field, the gas pressure inside the front should be constant, while the exterior pressure should decrease from the leading edge to the side according to the Bernoulli equation. Therefore, the front shape could not be stable. The gravitational potential of the dark matter halo allows a stable non-constant pressure distribution of the interior gas to emerge. It also provides stability against the global perturbations of the front shape. Indeed, let the front bend so that its curvature increases. The exterior pressure at the outskirts will decrease because the flow speed increases. At the same time, the interior pressure will increase since the front will be at a deeper gravitational potential level. The resulting pressure difference will restore the original front shape.

The presence of the massive dark halo is necessary also for suppression of the small-scale Rayleigh-Taylor instabilities. Due to ram pressure of the ambient gas, the cold cloud slows down, which leads to the effective gravity force directed from the inside of the cold front outward. Since the ambient gas density is lower, this configuration is unstable. Let us make numerical estimates. The drag force on the cloud is $F_\mathrm{d} = C \times \rho_\mathrm{out} v^2 A/2$, where ρ_out is the density of the ambient gas, A is the cloud cross-section area, and $C \approx 0.4$ is the drag coefficient for a cylinder with a rounded head at transonic speed. The cloud acceleration is then

$$g_\mathrm{d} = \frac{F_\mathrm{d}}{M} \approx \frac{0.2\,\rho_\mathrm{out} v^2 \pi r^2}{4/3\,\pi r^3 \rho_\mathrm{in}} = 0.15 \frac{\rho_\mathrm{out}}{\rho_\mathrm{in}} \frac{v^2}{r} \qquad (2)$$

Substitution of numerical values yields $g_\mathrm{d} \approx 8 \times 10^{-10}$ cm s^{-2}. At the same time, the gravitational accel-

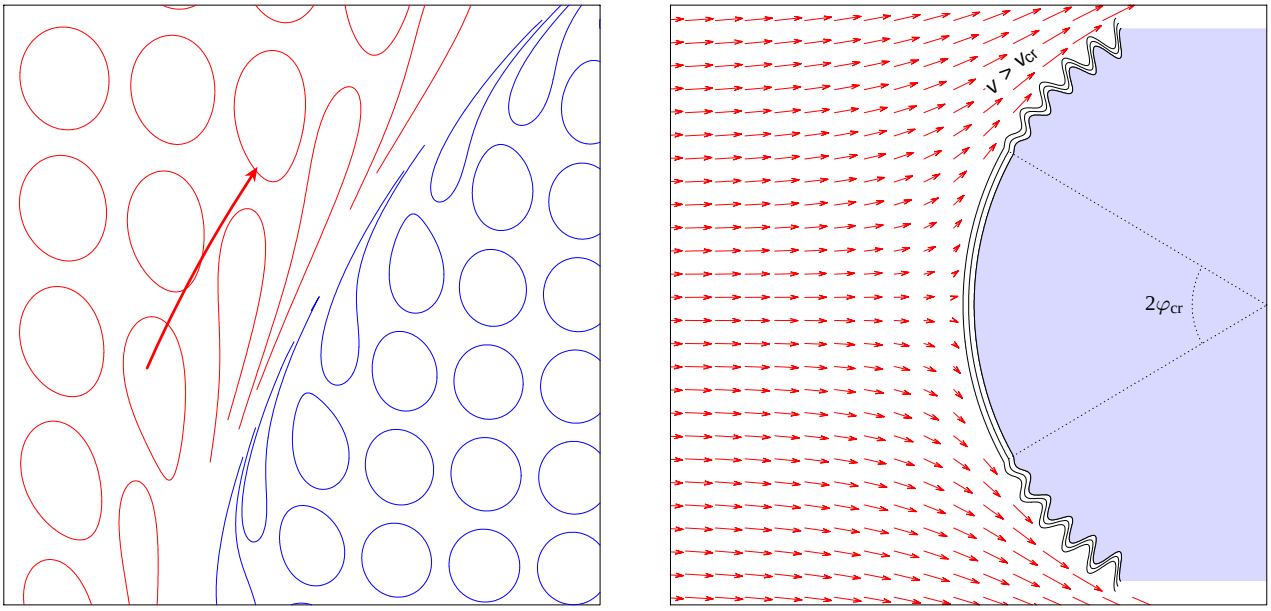

Fig. 7. *(a)* Illustration of the formation of the magnetic layer near the front surface. The initially tangled magnetic lines in the ambient hot gas (red) are stretched along the surface because of tangential motion of the gas. The magnetic lines inside the front are stretched because, in the absence of complete magnetic isolation, the cool gas experiences stripping. This process can form a narrow layer in which the magnetic field is parallel to the front surface. Such a layer would stop the transport processes across the front, as well as further stripping of the cool gas. *(b)* The interface between the cool and hot gas is subject to the Kelvin-Helmholtz instability. The magnetic layer can suppress this instability in the region where the tangential velocity is smaller that a critical value $v_{\rm cr}$. The velocity field shown for illustration corresponds to the flow of incompressible fluid around a sphere.

eration near the front due to the subcluster mass is

$$g = \frac{GM(<100\,\mathrm{kpc})}{(100\,\mathrm{kpc})^2} = 6.4\times10^{-9}\,\mathrm{cm\ s^{-2}}, \qquad (3)$$

acting in the opposite direction, and therefore the acceleration due to drag is negligible. Note that in the absence of dark matter, the gravitational acceleration (due to the gas only) would be a factor of 15 smaller, which is insufficient to compensate the drag acceleration. Therefore a purely gas could would be Rayleigh-Taylor unstable, as is indeed seen in numerical experiments (Jones et al. 1996).

MAGNETIC STRUCTURE NEAR THE COLD FRONT

Magnetic fields can profoundly affect the properties of the intergalactic medium (IGM) in clusters. The current measurements of intracluster magnetic fields are based on Faraday rotation in radio sources seen through the IGM (e.g., Kim, Kronberg & Tribble 1991), or on combined radio and hard X-ray data on cluster radio halos under the assumption that the X-rays are produced by inverse Compton scattering of the microwave background (e.g., Fusco-Femiano et al. 2000). Both these methods indicate the magnetic field strength on the microgauss level, with considerable uncertainty. The properties of the cold front in A3667 allow to determine the magnetic field strength by a completely new method, from its effect on dynamics of the intracluster gas.

The idea is as follows. We have seen that the cold front is very sharp and has a smooth shape; therefore, it must be mechanically stable. At the same time, it can be shown that given the observed velocity of the ambient gas flow, the sharp front must be rapidly destroyed by the Kelvin-Helmholtz instability. An examination of the possible mechanisms for the suppression of this instability points to the magnetic field surface tension as the most probable candidate.

The required magnetic field configuration can form through a scenario schematically shown in Fig. 7. An initially random magnetic field is frozen in the intracluster gas. Because of the tangential plasma motions around the front, the magnetic loops are stretched along the surface. The magnetic reconnection can then produce a layer in which the field lines are parallel to the interface between the cold and hot gases and to the flow. This configuration of the magnetic field also provides surface tension that can suppress the KH instability.

The flow speed increases as a function of distance from the cold front. If the magnetic field is not too strong, sooner or later it will be unable to stabilize the KH perturbations, and at this point the instabilities will start to grow; the location of this point is marked as $\varphi_{\rm cr}$ is Fig. 7. We expect that within the sector $\pm\varphi_{\rm cr}$ is sharp, while beyond it, the cloud boundary is smeared by turbulence. One readily notes the analogy with the X-ray image of A3667, where the front is sharp within $\varphi \approx 30^\circ$ and quickly smears beyond this radius (Fig. 1). Assuming that at $\varphi = 30^\circ$, the magnetic field tension is just enough to provide mechanical stability, we can determine the magnetic field strength.

Let us consider in detail the line of argument. For simplicity, we assume that the front velocity is $M = 1$ exactly.

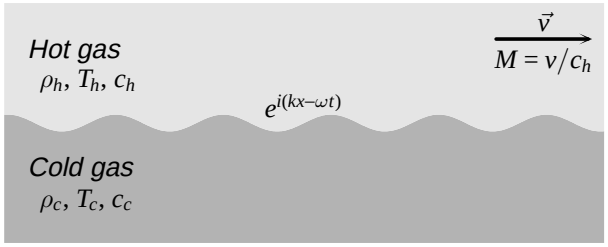

Fig. 8. Hot gas flows with a velocity $\vec{v}$ relative to the colder, denser gas. The interface is subject to the planar wave perturbations, $\exp(i(kx-\omega t))$, with the wave vector parallel to the flow. For the given wave vector, ω can be found from the dispersion equations: (5) for pure hydrodynamic and (13) in MHD.

Hydrodynamic KH instability of the cold front

The interface between two fluids in most cases is subject to two types of hydrodynamic instability: (i) Rayleigh-Taylor instability, which arises if the effective gravity is directed from the heavier fluid into the lighter one; and (ii) Kelvin-Helmholtz instability, which arises from tangential motion of the fluids. As was discussed above, the dark matter halo moving with the front suppresses the Rayleigh-Taylor instability. Therefore, we consider below only the KH instability.

A numerical solution of the $M = 1$ flow about the cold front gives the following angular dependence of the velocity of the ambient gas near the front:

$$M(\varphi) \simeq 1.1 \sin\varphi. \quad (4)$$

At $\varphi = 30^\circ$ the Mach number reaches $M = 0.55$. Clearly, this is a high velocity and therefore one expects a fast growth of the KH perturbations leading to formation of a turbulent layer. Below, we will use the following widely known properties of the KH instability: 1) The fastest-growing perturbations are parallel to the flow; 2) The short-wavelength modes grow faster than the long-wavelength modes; 3) The perturbations grow exponentially, and therefore a nonlinear stage is reached rapidly. When the nonlinear stage is reached, the amplitude is approximately equal to the wavelength of the initially linear perturbation; subsequently, the perturbations with a given wavelength merge into large vortices. Thus, if one can show that the perturbations with wavelength λ are unstable, the turbulent layer of width at least λ is expected.

Dispersion equation

The stability analysis is conveniently performed via consideration of the small perturbation of the interface in the form of the planar waves and solving the resulting dispersion equation. In our case the dispersion equation can be written as (Miles 1958):

$$-\frac{1}{\omega^2} - \frac{c_h^2/c_c^2}{(\omega - Mc_h k)^2} + \frac{1}{k^2 c_c^2} = 0, \quad (5)$$

where M is the Mach number of the hot gas, and c_c and c_h sound speeds in the cold and hot gases, respectively (see Fig. 8).

Application to A3667

For all relevant Mach numbers, equation (5) has two complex solutions for ω, one of them corresponding to the growing mode. The instability growth time is $\tau = (\mathrm{Im}\,\omega)^{-1}$. Although perturbations with any wavelength are formally unstable, only for some of them the growth time is sufficiently short compared to the lifetime of the front. The relevant time scale with which τ should be compared is the cluster core passage time, $t_{\rm cross} = L/M_\infty c_\infty$, where L is the cluster size. The value of $\exp(t_{\rm cross}/\tau)$ is the perturbation growth factor over the core passage time; if $t_{\rm cross}/\tau \gg 1$ (we will use a conservative fiducial threshold of 10), the perturbation is effectively unstable because it has enough time to become non-linear.

For the observed gas parameters and $M_\infty = 1$ the solution of (5) is approximately given by $t_{\rm cross}/\tau \simeq 12 ML/\lambda$, where $\lambda = 2\pi/k$ is the perturbation wavelength. Using the distribution of the Mach number near the front (eq. 4), we have[3]

$$\frac{t_{\rm cross}}{\tau} \simeq 3.3 \frac{L}{\lambda} \sin\varphi. \quad (6)$$

This equation, applied for a typical cluster size of $L =$ 1 Mpc, implies that perturbations with $\lambda = 10$ kpc are unstable ($t_{\rm cross}/\tau = 10$) at $\varphi > 1.7^\circ$, that is, essentially everywhere; at $\varphi = 10^\circ$, the modes with $\lambda < 57$ kpc are unstable, and at $\varphi = 30^\circ$, modes with $\lambda < 150$ kpc.

There is another effect which limits the lifetime of perturbations. The linear perturbations have non-zero group velocity $v_{\rm dr} = d\mathrm{Re}\,\omega/dk$, and therefore drift along the flow as they grow. In principle, in some cases the perturbation can move to the side of the front before it grows non-linear. A detailed analysis of solutions of eq. (5) shows that ω is always proportional to k and therefore the group velocity equals the phase velocity, $v_{\rm dr} = \mathrm{Re}(\omega)/k$. Furthermore, in the entire range of the flow velocities near the cold front in A3667, the imaginary part of ω is almost proportional to its real part:

$$\frac{\mathrm{Re}\,\omega}{\mathrm{Im}\,\omega} \simeq 0.70. \quad (7)$$

This equation implies a simple relation between the per-

[3]We note that the analogous equation (4) in Vikhlinin et al. 2001b contained a factor of $(2\pi)^2$ smaller numerical factor due to an algebraic error.

turbation growth factor and its displacement, $\Delta\varphi$:

$$\begin{aligned}&\text{Growth factor} = \\ &\exp\left(\int \mathrm{Im}\,\omega\, dt\right) \simeq \exp\left(1.43\int \mathrm{Re}\,\omega\, dt\right) = \\ &= \exp\left(1.43k\int \frac{\mathrm{Re}\,\omega}{k}\, dt\right) = \exp\left(1.43k\int dl\right) = \\ &\exp\left(4.7\frac{R}{\lambda}\frac{\Delta\varphi}{30^\circ}\right),\end{aligned} \tag{8}$$

where R is the radius of the front. Assuming, as before, that reaching a growth factor of e^{10} is required for a perturbation to become non-linear, we obtain the following condition for effective instability for $R = 410$ kpc:

$$\lambda < 190\,\mathrm{kpc}\,\frac{\Delta\varphi}{30^\circ}. \tag{9}$$

The longer wavelength perturbations drift to the side of the front before they grow non-linear. Perturbations with the interesting $\lambda \sim 30$ kpc should grow strongly non-linear before they leave the observed smooth region of the front.

To summarize, the perturbations with $\lambda \lesssim 30$ kpc are KH-unstable over most of the front surface, and therefore a formation of the turbulent layer of at least this width is expected. Since the observed front width is < 5 kpc (Vikhlinin et al. 2001a), the KH instability must be suppressed.

The commonly known mechanisms for suppression of the KH instability are a) gravity and b) surface tension at the interface. Let us consider them in application to A3667.

The role of gravity in suppressing the KH instability

As we showed above, there is a massive subcluster traveling with the front and its gravity has some stabilizing effect on the front. The gravitational force suppresses the KH instability if it acts in the direction from the lighter fluid into the heavier one, and if the following stability condition is satisfied:

$$\frac{g}{k} > v^2\,\frac{\rho_c\,\rho_h}{\rho_c^2-\rho_h^2}. \tag{10}$$

It is clear from this equation that only the long wavelength modes are suppressed by gravity, while the shorter wavelength perturbations can grow almost freely. Noting that $\rho_c \gg \rho_h$, equation (10) can be rewritten as

$$\frac{g}{k} \gtrsim v^2\frac{\rho_h}{\rho_c} = v^2\frac{T_c}{T_h} = v^2\frac{T_c}{c_s^2\,\mu m_p/\gamma} = \frac{T_c}{\mu m_p/\gamma}M^2. \tag{11}$$

The gravitational acceleration in the front rest frame was derived above. Using its numerical value, we obtain the following stability condition:

$$\frac{\lambda}{1\,\mathrm{kpc}} > 3500\,M^2 = 4200\,\sin^2\varphi \tag{12}$$

This implies that the perturbations with $\lambda = 10$ kpc are stabilized by gravity only within the sector $\varphi < 3^\circ$; at $\varphi = 5^\circ$ stability is achieved only for $\lambda > 32$ kpc, and at $\varphi = 30^\circ$ — for $\lambda > 1050$ kpc.

Therefore, gravity cannot suppress a formation of a turbulent layer with a width of 10–20 kpc. This leaves the surface tension of the magnetic field as the most likely mechanism for suppression of the KH instability.

Suppression of the KH instability by magnetic field

The KH instability can be suppressed by the surface tension of a magnetic field, if the latter is parallel to the interface and to the direction of the flow. We have discussed above that even if the magnetic field is initially highly tangled, the tangential gas motion near the front can create the required magnetic configuration (see. Fig. 7).

The analysis of KH instability in MHD is greatly simplified if the plasma can be considered incompressible. Fortunately, this can be done in our case because the gas exterior to the front flows with a relatively low local Mach number $M \lesssim 0.5$, and the growing modes of the KH instability in the interior cool gas generally have low phase speed. The incompressibility assumption can be also justified by the fact that the growth time of the hydrodynamic instability given by eq. (5) is very close to that in the incompressible limit, i. e. for $Mc_h \to v$, $c_c/c_h^2 \to \rho_h/\rho_c$, $c_c \to \infty$.

The dispersion equation for small perturbations in a perfectly conducting, incompressible plasma can be written as (Syrovatskij 1953)

$$\rho_h(\omega - kv)^2 + \rho_c\omega^2 = k^2\left(\frac{B_h^2}{4\pi} + \frac{B_c^2}{4\pi}\right) \tag{13}$$

where B_h and B_c are the magnetic field strengths in the hot and cold gas, respectively (we assume that the field lines are elongated with the flow), and ρ_h and ρ_c are the gas densities. The solutions of this equation are real (the interface is stable) if

$$B_h^2 + B_c^2 > 4\pi\,\frac{\rho_h\,\rho_c}{\rho_h+\rho_c}\,v^2. \tag{14}$$

Application to A3667

If the magnetic pressure is small compared to the thermal pressure, p (as it turns out to be the case), or is the same fraction of p on both sides of the interface, the stability condition (14) can be rewritten in terms of the thermal pressure and temperature of the gas:

$$\frac{B_h^2}{8\pi} + \frac{B_c^2}{8\pi} > \frac{1}{2}\,\frac{\gamma M^2}{1+T_c/T_h}\,p_{\mathrm{gas}}. \tag{15}$$

Therefore, for the observed temperatures and flow velocities the stability of the cold front within the sector $\varphi < 30^\circ$, where $M \leqslant 0.55$, requires that $(B_h^2+B_c^2)/8\pi > 0.17p$. If smearing of the front beyond this sector is interpreted as the onset of the instability, this becomes an estimate of the total magnetic pressure:

$$p_{\mathrm{mag},h} + p_{\mathrm{mag},c} = 0.17\,p_{\mathrm{gas}} \tag{16}$$

The formal statistical uncertainty in the derived value of the magnetic field strength is mostly due to uncertainty in the angle, $\varphi_{\rm cr}$, where the interface becomes unstable, and hence in the local Mach number of the hot gas. For $\varphi_{\rm cr}$ in the range $30^\circ \pm 10^\circ$ (which appears to be a conservative interval, see Fig. 1), we find from eq. (14) and (4) that the magnetic field strengths are in the interval

$$0.09p < \frac{B_h^2+B_c^2}{8\pi} < 0.23p. \qquad (17)$$

The maximum of the magnetic field strengths in the cold and hot gases, $B = \max(B_h, B_c)$, is in the interval $(4\pi p_{\rm mag})^{1/2} < B < (8\pi p_{\rm mag})^{1/2}$, where $p_{\rm mag} = (B_h^2+B_c^2)/8\pi$ is constrained by (17). Using the value of gas pressure inside the dense cloud, we find the corresponding uncertainty interval $7\,\mu{\rm G} < B < 16\,\mu{\rm G}$.

Thus, the front sharpness near the axis and its gradual smearing at large angles are most likely explained by the existence of a layer with a ~ 10 μG magnetic field parallel to the front. Equation (16) shows that the magnetic pressure in the layer is a small fraction of the gas pressure. Everywhere else it should be even smaller, because the magnetic field in the layer is amplified by stretching of the field lines. This conclusion is robust: e.g., if the magnetic pressure were of order of the thermal pressure, eq. (15) implies that the front would be stable for Mach numbers up to $M \sim 1.9$, i.e. over the entire surface of the cool gas cloud.

Faraday rotation measurements of the magnetic field outside the cluster cooling flows provide the values of B from ~ 1 μG (Kim et al. 1991) to ~ 10 μG (Clarke et al. 2000), with considerable uncertainty of the absolute field strength due to unknown degree of entanglement. Near the cold front, the field is straightened and amplified, so our estimate likely is an upper limit on the absolute field strength in the cluster core, and thus is consistent with the Faraday rotation measurements in the bulk of IGM.

Note that to suppress the instability, the magnetic field does not have to be completely ordered. It is sufficient to arrange for uniformity on the scales of order 100 kpc. The perturbations with $\lambda < 10$ kpc will then stabilized, while the growth time for perturbations with$\dot{\lambda} > 100$ kpc is longer than the front lifetime anyway.

The stretching of magnetic field lines by tangential plasma motions is not the only mechanism for creation of a layer with a highly ordered magnetic field. For example, Frank et al. (1996) and Jones et al. (1997) showed that even a weak seed magnetic field which is incapable of suppressing the KH instability, is significantly amplified in the nonlinear vortices, and after active field line reconnections, a thin layer is formed. In this layer, the field lines are aligned with the flow and the field strength increases so that interface becomes stable. Therefore, the formation of a magnetic layer considered above seems natural; once formed, the layer acts as "magnetic isolation" which stops the transport processes across the front, and also as "magnetic lubrication", which provides for nonviscous, laminar flow around the cold front.

In conclusion, we note that the structures similar to the cold fronts in A3667 and A2142 have now been detected in many other clusters; this is a rather common phenomenon (see Markevitch et al. 2002 for a review).

We thank P. Mazzotta for pointing out an algebraic error in derivation of equation (6).

REFERENCES

[1] Blondin, J. M. 1994, ApJ, 435, 756
[2] Frank, A., Jones, T. W., Ryu, D., Gaalaas, J. B., 1996, ApJ, 460, 777.
[3] Fusco-Femiano, R., dal Fiume, D., Feretti, L., Giovannini, G., Grandi, P., Matt, G., Molendi, S., Santangelo, A., 1999, ApJ, 513, L21.
[4] Joffre, M., Fischer, P., Frieman, J., et al., 2000, ApJ, 534, L131.
[5] Jones, T. W., Ryu, D., Tregillis, I. L., 1996, ApJ, 473, 365.
[6] Jones, T. W., Gaalaas, J. B., Ryu, D., Frank, A., 1997, ApJ, 482, 230.
[7] Katgert, P., Mazure, A., den Hartog, R., Adami, C., Biviano, A., Perea, J., 1998, A&AS, 129, 399.
[8] Kim, K. ., Kronberg, P. P., Tribble, P. C., 1991, ApJ, 379, 80.
[9] Knopp, G. P., Henry, J. P., Briel, U. G., 1996 ApJ, 472, 125.
[10] Miles, J. W., 1958, J. Fluid Mech., 4, 538
[11] Markevitch, M., Ponman, T. J., Nulsen, P. E. J., et al., 2000, ApJ, 541, 542.
[12] Markevitch, M., Vikhlinin, A., Forman, W., 2002, astro-ph/0208208
[13] Sodre, L. J., Capelato, H. V., Steiner, J. E., Proust, D., Mazure, A., 1992, MNRAS, 259, 233.
[14] Syrovatskij, S. I., 1953, JETP, 24, 622
[15] Röttgering, H. J. A., Wieringa, M. H., Hunstead, R. W., Ekers, R. D., 1997, MNRAS, 290, 577.
[16] Vikhlinin, A., Markevitch, M., Murray, S. S., 2001a, ApJ, 551, 160.
[17] Vikhlinin, A., Markevitch, M., Murray, S. S., 2001b, ApJ, 549, L47.